

LoXR: Performance Evaluation of Locally Executing LLMs on XR Devices

Dawar Khan[✉], Xinyu Liu, Omar Mena[✉], Donggan Jia[✉], Alexandre Kouyoumdjian[✉], Ivan Viola[✉]

Abstract—The deployment of large language models (LLMs) on extended reality (XR) devices has great potential to advance the field of human-AI interaction. In case of direct, on-device model inference, selecting the appropriate model and device for specific tasks remains challenging. In this paper, we deploy 17 LLMs across four XR devices—Magic Leap 2, Meta Quest 3, Vivo X100s Pro, and Apple Vision Pro—and conduct a comprehensive evaluation. We devise an experimental setup and evaluate performance on four key metrics: performance consistency, processing speed, memory usage, and battery consumption. For each of the 68 model-device pairs, we assess performance under varying string lengths, batch sizes, and thread counts, analyzing the tradeoffs for real-time XR applications. We finally propose a unified evaluation method based on the Pareto Optimality theory to select the optimal device-model pairs from the quality and speed objectives. We believe our findings offer valuable insight to guide future optimization efforts for LLM deployment on XR devices. Our evaluation method can be followed as standard groundwork for further research and development in this emerging field. All supplemental materials are available at nanovis.org/Loxr.html.

Index Terms—Extended reality, large language models, human AI interactions, performance evaluation, conversational user interfaces

1 INTRODUCTION

SINCE the 2022 release of OpenAI’s ChatGPT interface [1], relying on the GPT-3.5 Large Language Model (LLM), we have witnessed the disruptive and transformative effects of LLMs. These models are capable of describing a wide variety of topics, respond at various levels of abstraction, and communicate effectively in multiple languages. They have proven capable of providing users with accurate and contextually appropriate responses. LLMs have quickly found applications in tasks such as spelling and grammar correction [2], generating text on specified topics [3], integration into automated chatbot services, and even generating source code from loosely defined software specifications [4].

Research on language models, and on their multimodal variants integrating language and vision or other technologies has recently experienced rapid growth. For instance, in computer vision, language models are combined with visual signals to achieve tasks such as verbal scene description and even open-world scenegraph generation [5]. These technologies enable detailed interpretation of everyday objects, inference of relationships among them, and estimates of physical properties like size, weight, distance, and speed. In user interaction and visualization research, LLMs serve as verbal interfaces to control software functionality or adjust visualization parameters [6], [7]. Through prompt engineering or fine-tuning, loosely defined text can be translated into specific commands that execute desired actions within a system, supported by language model APIs. The capabilities of language models continue to improve significantly from one version to the next. Yet,

this comes at the cost of a significant growth in size of the most advanced models. As an example, models released or operated by leading companies such as OpenAI, Meta, Microsoft, and Google now reach the scale of trillions of trainable parameters [1]. Due to their size and complexity, the training and inference of these models are limited to dedicated data centers equipped with considerable computational and memory resources.

Another disruptive application of LLMs involves their use in wearable technology to assist users in various environments. For instance, Meta AI is being integrated into Meta’s virtual reality hardware, where images captured by the device are streamed over the network to Meta’s servers for model inference, enabling image interpretation or prompt response tasks.¹ The overarching vision is to develop assistive hardware that is as lightweight as sunglasses but capable of aiding users in a wide range of tasks by understanding the scene they are viewing.

While such technological advances have the potential to empower users in unprecedented ways, three main drawbacks must be considered due to the heavy reliance on network connectivity and cloud-based data processing. First, users will need to maintain *extremely high network connectivity* to ensure that remote services can perform assistive tasks without excessive latency, which would degrade the user experience. Second, *data privacy* poses a significant challenge. Many environments, such as medical settings and various industries, operate under strict data privacy regulations that prohibit the transmission of sensitive information to remote servers, precluding the use of these services in such contexts. Third, the reliance on *subscription models* for these assistive services introduces ongoing costs for users, requiring them to periodically purchase licenses, which can accumulate into significant long-term costs.

Therefore, there is dedicated research effort focused on developing autonomous AI assistive technologies that can perform inference directly on a device. To this goal, several smaller

- Dawar Khan, Omar Mena, Donggan Jia, Alexandre Kouyoumdjian, Ivan Viola are with King Abdullah University of Science and Technology (KAUST), Saudi Arabia. E-mail: {xinyu.liu, dawar.khan, omar.mena, donggan.jia, alexandre.kouyoumdjian, ivan.viola}@kaust.edu.sa.
- Xinyu Liu is with King Abdullah University of Science and Technology (KAUST), Saudi Arabia, and also with University of Electronic Science and Technology of China, Chengdu, China.
- D. Khan and X. Liu are joint first authors with equal contributions.

Manuscript received MM dd, YYYY; revised MM dd, YYYY.
(Corresponding author: Dawar Khan.)

1. <https://www.meta.com/blog/quest/meta-ai-on-meta-quest-3/>

LLMs have been released by Meta, Mistral AI, Microsoft, and Google [8]. These models are designed to potentially operate on mobile devices or extended reality hardware and are typically around billions of trainable parameters in size. Some LLMs with fewer than a billion trainable parameters have shown very good results [8].

Local execution of LLMs on XR devices is expected to become increasingly necessary for a wide range of applications, particularly those that require real-time processing and device autonomy. However, selecting the optimal device and model for a specific application is a complex decision: device specifications and model documentation alone are not sufficient for making it, as the performance of most LLMs running on various hardware components remains largely undocumented. Furthermore, the hardware configurations of XR devices (such as CPU, memory capacity, and thermal management) and the architectures of the LLMs can significantly influence the results. Therefore, defining standardized evaluation criteria that address these complexities and ensures fairness across tests is also a research challenge. To the best of our knowledge, no comprehensive study currently provides clear guidelines for such evaluations.

To address these challenges, we present LoXR, a comprehensive study deploying LLMs on XR, focusing on performance evaluation across various metrics. Considering the multiple challenges and factors affecting the evaluation, we first identify key evaluation metrics, and then design an experimental setup to minimize potential bias. Specifically, we deploy 17 LLMs across four XR devices—Magic Leap 2, Meta Quest 3, Vivo X100s Pro², and Apple Vision Pro—and conduct a thorough evaluation in terms of performance consistency i.e., stability over time, processing speed, memory usage, and battery consumption. This results in 68 model-device pairs. A key challenge is the effect of varying string lengths, batch sizes, thread counts, and background processes. To account for string length variation, we conducted experiments using different lengths. To mitigate hidden factors like background processes, each experiment was repeated five times, and average values were calculated. To provide task-specific analysis, experiments were conducted across all LLMs tasks: Prompt Processing (PP) for evaluating performance with varying prompt lengths, Token Generation (TG) for varying generated token set sizes, plus Batch Test (BT) and Thread Test (TT) for assessing parallelism and concurrency efficiency. We believe our experimental protocol and results will serve as a foundation for further research and development in this emerging field.

In summary, this paper contributes:

- An evaluation approach and an experimental setup for assessing the performance of LLMs on XR devices, that can be used as standard guidelines for future research.
- The deployment of 17 LLMs on four XR devices, and a comprehensive evaluation, resulting in 68 model-device pairs, across five critical metrics: consistency, processing speed, concurrency and parallelism, memory usage, and battery consumption.

2 RELATED WORK

We review related work with respect to two major research directions. The first research direction is exploring the use of

² Vivo X100s Pro is strictly speaking not an XR device. We include it in our comparison because smartphones are commonly used as XR devices, and this device features competitive hardware specifications in the market.

LLMs on XR devices, and the second research direction explores how to make LLMs directly deployable on low-resource hardware.

2.1 LLM-powered XR Applications

Owing to the powerful semantic understanding and extensive general knowledge of LLMs, numerous studies have explored their application in assisting various tasks within XR scenarios.

Torre *et al.* [9] introduced *LLMR*, a framework that leverages LLMs for the real-time creation and modification of interactive mixed reality experiences, enabling tasks such as generating new content or editing existing works on VR/AR devices. Jia *et al.* [6] developed the *VOICE* framework, which employs a two-layer agent system for conversational interaction and explanation in scientific communication, with a prototype deployable on VR devices. Kurai *et al.* [10] proposed *MagicItem*, a tool that allows users with limited programming experience to define object behaviors within the metaverse platform. Zhang *et al.* [11] introduced *OdorAgent*, which combines an LLM with a text-image model to automate video-odor matching. Yin *et al.* [12] identified potential limitations in LLM-based automated systems and proposed the systematic framework *Text2VRScene* to address them. Chen *et al.* [13] leveraged the extensive capabilities of LLMs in context perception and text prediction to enhance text entry efficiency by reducing manual keystrokes in VR scenarios. Giunchi *et al.* [14] developed *DreamCodeVR*, a tool designed to help users, regardless of coding experience, create basic object behavior in VR environments by translating spoken language into code within an active application. Wan *et al.* [15] presented an LLM-based AI agent for human-agent interaction in VR, involving GPT-4 to simulate realistic NPC behavior, including context-aware responses, facial expressions, and body gestures.

As they stand, these previous contributions still require the deployed devices to connect to a cloud server for LLM inference, raising concerns about user privacy, latency, costs, and internet access requirements. In our work, we evaluate the local inference performance of various LLMs and propose a prototype capable of using local LLM inference.

2.2 On-device LLMs

Running LLMs on edge devices, commonly called on-device LLMs, has garnered significant research interest due to their advantages in enhancing privacy, reducing latency, and operating without the need for internet connectivity. Because of the limited memory and computing capabilities, on-device LLMs usually require resource-efficient LLM deployment [16]: a trade-off between performance and model size.

Cheng *et al.* [17] introduced the *SignRound* method, which leverages signed gradient descent to optimize both rounding values and weight clipping. This approach achieves outstanding performance in 2- to 4-bit quantization while maintaining low tuning costs and eliminating additional inference overhead. Ma *et al.* [18] developed the *LLM-Pruner* method, which uses structural pruning to selectively remove non-essential coupled structures based on gradient information, effectively preserving the core functionality of the LLM. Their results demonstrate that the compressed models continue to perform well in tasks such as zero-shot classification and generation. Gu *et al.* [19] introduced a novel knowledge distillation method that compresses LLMs into smaller models, resulting in the student model *MINILLM*. *MINILLM* demonstrates superior performance compared to baseline models, producing

more precise responses with reduced exposure bias, improved calibration, and enhanced long-text generation capabilities. Liu *et al.* [20] developed a tuning-free 2-bit KV cache quantization algorithm, named *KIVI*, which independently quantizes the key cache per channel and the value cache per token. This approach enabled up to a 4× increase in batch size, resulting in a 2.35× to 3.47× improvement in throughput on real LLM inference workloads. Liu *et al.* [21] introduced *MobileLLM*, which explores the importance of model architecture for sub-billion-parameter LLMs by leveraging deep and narrow architectures, combined with embedding sharing and grouped-query attention mechanisms.

Although these studies primarily focused on reducing model size efficiently for deployment on various devices, they did not evaluate the models’ performance in real-world on-device scenarios, which is the focus of our paper.

3 RESEARCH METHODS AND MATERIALS

The aim of this study is to deploy LLMs on XR devices and evaluate their performance in different aspects. This section outlines our research methodology, including the key challenges, the LLM deployment approach, and the evaluation metrics and models used in this study.

Problem Statement: In this study, we deploy 17 LLMs, denoted as $\{m_1, m_2, \dots, m_{17}\}$ (see Table 1), across four XR and mobile devices: d_1, d_2, d_3 , and d_4 , representing Magic Leap 2 (ML2),³ Meta Quest 3 (MQ3),⁴ Vivo X100 Pro (Vivo),⁵ and Apple Vision Pro (AVP),⁶ respectively. Our goal is to perform a comprehensive evaluation of these models on the four devices to determine how well they handle large-scale language processing tasks in resource-constrained XR environments.

We define our evaluation using six key performance metrics: $p_0, p_1, p_2, p_3, p_4, p_5$, which represent *Model Quality*, *Performance Consistency*, *Performance Speed* (with respect to string length and prompt length), *Parallelism* (with respect to thread count and varying batch size), *Memory Usage*, and *Battery Usage*, respectively.

Each LLM $m_i \in \{m_1, m_2, \dots, m_{17}\}$ is tested on each XR device $d_j \in \{d_1, d_2, d_3, d_4\}$ for evaluation across each performance metric $p_k \in \{p_0, p_1, p_2, p_3, p_4, p_5\}$. The evaluation can be summarized as X_{mdk} , as given in Eq. (1).

$$X_{mdk} = \{x_{ijk} \mid i \in \{1, \dots, 17\}, j \in \{1, \dots, 4\}, k \in \{0, \dots, 5\}\} \quad (1)$$

Here, x_{ijk} represents the performance of model m_i on device d_j for metric p_k , forming the basis for cross-device and cross-model analysis.

Fig. 1 presents an overview of our research pipeline, where each rectangular box represents a specific procedure, and the connected ovals indicate their respective outcomes. These are discussed in detail below.

3.1 LLM Deployment on XR Devices

We aim to deploy the LLMs locally on XR devices. For this purpose, we customize the Llama.cpp library [22] and build it for the four target XR devices. The resulting application is capable of loading various appropriately sized GPT-Generated Unified

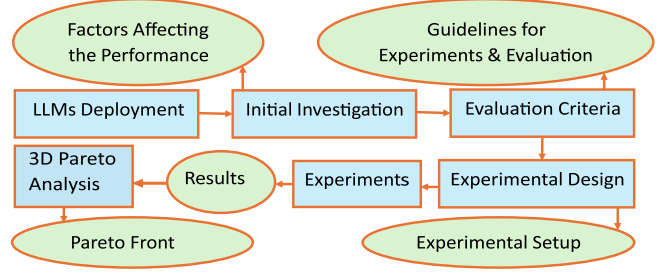


Fig. 1. Overview of our research process. The rectangular boxes represent the procedures, while the ovals indicate the outcomes. We deployed 17 LLMs on four XR devices. First, we identified the key factors affecting performance. Based on these factors, we defined our evaluation criteria and conducted the experiments. Finally, we applied 3D Pareto analysis, which provided the Pareto front to highlight the best-performing model-device pairs.

Format (GGUF) models. Our deployment leverages the functionalities of *Llama*, allowing us to run basic LLMs tasks, and adjust various parameters. For example, to evaluate different aspects in an experiment, we can control various parameters such as prompt length in *Prompt Processing* (PP) and the size of the token set in *Token Generation* (TG). To benchmark the models on various devices, the top-level scripts in Llama.cpp are compiled into binary executable files. These binaries include scripts specifically designed for testing both execution speed and model quality. For Apple Vision Pro, we utilized Xcode⁷, Apple’s official IDE, to build and deploy testing scripts directly to the device. For the remaining three devices, the testing was performed via a shell interface opened through Android Debug Bridge (ADB). In our current study, we selected 17 models, each running on the four chosen devices.

Due to compatibility constraints with Llama.cpp, we conducted testing exclusively on the CPU for Magic Leap 2, Meta Quest 3, and Vivo X100s Pro. As a smartphone, the Vivo X100s Pro theoretically supports GPU inference through frameworks like TensorFlow Lite or ONNX Runtime, but Llama.cpp does not currently offer GPU inference support for this device. Similarly, Magic Leap 2 and Meta Quest 3, being XR-specific devices, lack user-accessible GPU inference capabilities compatible with Llama.cpp. In contrast, Apple Vision Pro supports GPU inference via Metal, which we used in our experiments. These device and framework limitations necessitated restricting inference to CPUs for the first three devices.

3.2 Initial Investigation and Factors Identification

After deploying the LLMs, we conducted an initial investigation through anecdotal informal tests, literature reviews, and by studying LLM documentations. The aim of this preliminary investigation was to identify the key challenges and factors affecting performance—prerequisites for a fair evaluation—and to define our evaluation approach (Section 3.3).

We observed that XR devices experience performance degradation during prolonged tasks due to factors such as overheating, battery depletion, and background processes. Moreover, they often do not perform at a stable level. For instance, with the same model-device pair and parameters, we obtained different results across different runs of the same test. We refer to the metric used for measuring this variability as *Performance Consistency*. Another important

3. <https://www.magicleap.com/magicleap-2>

4. <https://www.meta.com/quest>

5. <https://www.vivo.com/en>

6. <https://www.apple.com/vision-pro>

7. <https://developer.apple.com/xcode/>

factor is execution time: the time taken to execute a particular task. In our context, we used a relative term called *Processing Speed*, measured in *tokens per second*. We observed variations in processing speed depending on varying string length, batch size, and thread count. In addition, *Memory Consumption* and *Battery Consumption* are also important factors to consider. Similarly, we observed different processing speeds for different tasks. For example, prompt processing and token generation exhibited varying performance, even with the same model-device pairs and parameters.

In addition to the parameters mentioned above, during the initial investigation, we also noticed that ensuring consistent testing conditions across devices is critical for fair comparisons but challenging to maintain. For example, variance in a device’s *Performance Consistency* could create biases into the results. LLM performance may vary due to different architectures and device-specific optimizations. Even with identical parameters, the same device and LLM can produce different results due to unknown factors. The device’s environment, such as exposure to heat or obstructions to the cooling fan, can also affect performance. The concise presentation of the findings, and ensuring their reproducibility for re-evaluation and validation, is an additional challenge. Considering these challenges, we formulated a set of guidelines as our evaluation approach in Section 3.3.

3.3 Evaluation Approach

Considering the key challenges and our initial investigation (see Section 3.2), we formulate a standardized evaluation approach for our assessments. First, we designed an experimental setup to minimize potential biases and ensure the validity of the results (see Section 4). This setup establishes identical parameters across all devices and defines the test types to be executed.

We developed several guidelines to ensure a comprehensive and standardized evaluation. To account for potential performance variations among LLMs, we selected 17 models from five different series (see Table 1) and evaluated them across four devices. Additionally, we conducted *Model Quality* analysis to provide technical insights into the selected models. These tests are device-independent, and were conducted to understand the details and properties of each model. Next, each model-device pair was subjected to various tests (see Section 3.4).

To mitigate performance fluctuations, each experiment was repeated multiple times, and the average results were computed. Finally, we unified the five evaluation metrics, i.e., $[P_1, P_5]$, using *Pareto Efficiency* theory to identify Pareto-optimal model-device pairs. Our evaluation framework and experimental design aim to facilitate reproducibility for other researchers. Additionally, we will provide open-source test scripts to enable replication of our study and further evaluations.

3.4 Models and Evaluation Metrics

We use 17 LLMs from five different series (see Table 1) in our evaluations. The models were obtained from Hugging Face’s model repository, a widely used platform for accessing pre-trained LLMs [23]. For consistency in naming conventions, we assigned unique IDs (m_1 to m_{17}) to these models.

Based on the *Llama* documentation [22] and our initial investigation, this evaluation comprises multiple tests to assess various performance parameters. For testing, we use *Synthetic Prompts* automatically generated by `llama.cpp`, ensuring uniform testing

TABLE 1
Models used, with their IDs, names, versions (v), quantization level (Q), layers (L), parameters (P), and sizes, sourced from Hugging Face [23].

Series	ID	Model Name	v	Q	L	P	Size	
Qwen	m_1	qwen2-0.5b-instruct-fp16	v2.0	FP16	24	0.5B	0.942 GB	
	m_2	Vikhr-Gemma-2B-instruct-Q3_K_M	v1.3	Q3	26	2.61B	1.36 GB	
	Vikhr-Gemma	m_3	Vikhr-Gemma-2B-instruct-Q4_0	v1.3	Q4	24	2.61B	1.51 GB
		m_4	Vikhr-Gemma-2B-instruct-Q5_0	v1.3	Q5	24	2.61B	1.75 GB
		m_5	Vikhr-Gemma-2B-instruct-Q6_K	v1.3	Q6	24	2.61B	2.00 GB
Phi-3.1	m_6	Phi-3.1-mini-4k-instruct-Q2_K	v3.1	Q2	20	3.82B	1.32 GB	
	m_7	Phi-3.1-mini-4k-instruct-Q3_K_L	v3.1	Q3	20	3.82B	1.94 GB	
	m_8	Phi-3.1-mini-4k-instruct-Q4_K_L	v3.1	Q4	20	3.82B	2.30 GB	
	m_9	Phi-3.1-mini-4k-instruct-Q5_K_L	v3.1	Q5	20	3.82B	2.68 GB	
	m_{10}	Phi-3.1-mini-4k-instruct-Q6_K	v3.1	Q6	20	3.82B	2.92 GB	
	m_{11}	Phi-3.1-mini-4k-instruct-Q8_0	v3.1	Q8	20	3.82B	3.78 GB	
LLaMA-2	m_{12}	llama-2-7b-chat.Q2_K	v2.0	Q2	28	6.74B	2.63 GB	
	m_{13}	llama-2-7b-chat.Q3_K_S	v2.0	Q3	28	6.74B	2.75 GB	
Mistral-7B	m_{14}	Mistral-7B-Instruct-v0.3.IQ1_M	v0.3	IQ1	28	7.25B	1.64 GB	
	m_{15}	Mistral-7B-Instruct-v0.3.IQ2_XS	v0.3	IQ2	28	7.25B	2.05 GB	
	m_{16}	Mistral-7B-Instruct-v0.3.IQ3_XS	v0.3	IQ3	28	7.25B	2.81 GB	
	m_{17}	Mistral-7B-Instruct-v0.3.IQ4_XS	v0.3	IQ4	28	7.25B	3.64 GB	

conditions without reliance on an external dataset. The string length is controlled via a parameter set to 64, 128, 256, 512, and 1024 tokens. The evaluation includes the following tests.

- **Performance Consistency:** Measures stability over time.
- **Processing Speed:** Analyzes performance across different string and prompt lengths, further divided into:
 - **PP (Prompt Processing):** Evaluates encoding efficiency in handling input prompts of varying lengths.
 - **TG (Token Generation):** Evaluates the device’s speed in generating output tokens of varying lengths.
- **Parallelization and Concurrency:** This includes:
 - **Batch Test (BT):** Evaluates the device’s ability to process multiple input samples simultaneously by handling different batch sizes during token generation.
 - **Thread Test (TT):** Measures performance scalability by varying thread counts during LLM execution.

Here, **Batch Size** refers to the number of input samples processed in parallel. While larger batch sizes improve computational efficiency, they also demand more memory. Each of these metrics requires task-specific analysis for both models and devices. Furthermore, we conducted additional evaluations for *Memory Usage* and *Battery Consumption*. Finally, we performed a **Pareto Optimality** analysis to collectively examine the results across different models and devices.

4 EXPERIMENTAL SETUP

This section describes the experimental setup and methodology for evaluating processing speed and error rates. The results are presented in Section 5. Before diving into the detailed setup, we first discuss the two evaluation metrics: processing speed and error count.

Processing Speed: In this study, we measure the processing speed for each model-device pair (m_i, d_j) by recording the time t_{ijk} taken by model m_i running on device d_j to process a string of length L . The instantaneous processing speed, $S_{inst.}$, expressed in tokens per second, is calculated as follows:

$$S_{inst.} = \frac{L}{t_{ij}}. \quad (2)$$

However, instead of relying on a single run, we perform 5 runs for each model-device pair to ensure accuracy and measure stability. If the coefficient of variance (CV) across the 5 runs is less than 40%, we calculate the 5-Run-Mean Speed (referred to as consistent speed, S_c) as:

$$S_c = \frac{1}{5} \sum_{k=1}^5 S_{\text{inst.}}(k), \quad (3)$$

where $S_{\text{inst.}}(k)$ represents the instantaneous speed during the k^{th} run of each experiment, calculated via Eq. (2). This approach minimizes the impact of factors such as initialization delays, hardware fluctuations, or other environmental inconsistencies, providing a more reliable measure of processing speed.

Error Count: If the CV exceeds 33%, the run is considered unstable, and the corresponding data point is excluded from further analysis. The count of such unstable runs is recorded as an error during the experiment.

We conducted the following four types of experiments.

4.1 Models Quality Analysis

Due to the storage and computational limitations of edge devices, deploying LLM locally often requires a trade-off between model size and performance. To put our performance results in perspective, we first conducted an empirical analysis of the models we have used in this study. This section offers insights into the models evaluated in this work, presenting a comparative analysis. While this section is not directly related to device performance, we believe providing detailed information about the models is essential for understanding their capabilities and limitations. We select six benchmarks to evaluate each model and calculate different metrics for each run:

- Hellaswag [24]: commonsense reasoning tasks, focusing on selecting the most plausible ending to a given situation from multiple options.
- mmlu [25]: evaluating a model’s knowledge and reasoning across 57 different subjects, ranging from elementary-level topics to advanced professional knowledge.
- ARC [26]: evaluating model’s ability to answer complex, grade-school science questions that require reasoning and problem-solving beyond simple fact retrieval.
- Truthful-qa [27]: evaluate how accurately AI models generate truthful answers to questions, especially in cases where common misconceptions or false information could lead to incorrect responses.
- winogrande [28]: large-scale benchmark for commonsense reasoning, specifically designed to test a model’s ability to resolve ambiguous pronouns in sentences.
- WikiText-2 [29]: containing over 100 million tokens, sourced from verified Wikipedia articles, designed to support research in language modeling and text generation tasks.

For the first five benchmarks, which consist of multiple-choice questions, we use accuracy as the evaluation metric. However, for WikiText-2, the task is to predict the probability of each word in a given text, reflecting the model’s natural language understanding. Therefore, we use perplexity as the evaluation metric, defined as:

$$\text{Perplexity}(P) = e^{-\frac{1}{N} \sum_{i=1}^N \log P(w_i)} \quad (4)$$

where $P(w_i)$ represents the probability assigned by the model to the i -th word, and N is the total number of words in the sequence.

4.2 Evaluating Performance Consistency

Some devices may experience performance degradation over time. In these experiments, we evaluate how processing speed fluctuates

across multiple runs. For each model m_i and device d_j , we perform N runs and compute the mean (μ_{ij}) of the speed (S_c), standard deviation σ_{ij} , and coefficient of variation (CV_{ij}). We also record the error count, as well as the maximum and minimum speeds observed during each experiment.

In our experiments, we set $N = 20$, i.e., each model-device pair is tested 20 times to evaluate performance variance. The mean speed across N runs is calculated as:

$$\mu = \frac{\sum_{i=1}^N S_c}{N}, \quad (5)$$

where S_c represents the 5-Run-Mean speed measured during each run, calculated as in Eq. (3). In other words, each S_c itself is the mean of 5 runs, ensuring that the measured value is not too affected by errors or hidden factors.

To let the devices cool down and conduct each run in comparable circumstances, we leave each device idle for two minutes between each run of the same model. We find this to be adequate, but just to be safer, between different models, we leave each device idle for ten minutes. We noted that the Meta Quest is not very prone to heating up. Heating was more noticeable on the Vivo X100s Pro, so it is always placed on a metal plate for heat dissipation. This is not representative of actual use, but this device is included in our evaluation as a baseline, not as an example of an actual XR headset. Magic Leap features a cooling fan, as does Vision Pro.

For each test, we conducted both PP and TG evaluations with the string length set to 64, i.e., PP = 64 and TG = 64. For each model-device pair, we calculated the standard deviation, mean, and CV. The results are presented in Section 5.2.

4.3 Processing Speed and String Length

String length, comprising both *Prompt Length* and *Size of the Token Set*, significantly affects performance. We evaluate the performance of LLMs on XR devices with varying string lengths to assess their processing speed. For each experiment, the processing speed is calculated as in Eq. (3).

We conducted experiments for five different string lengths (64, 128, 256, 512, and 1024) under the following PP and TG setups.

- **PP:** The PP values were set to 64, 128, 256, 512, and 1024, while TG was fixed at 0, with all other parameters set to their default values.
- **TG:** The TG values were set to 64, 128, 256, 512, and 1024, while PP was fixed at 0, with all other parameters set to their default values.

The results are shown in Section 5.3.

4.4 Parallelization with Thread Count and Batch Size

The parameters *Batch Size* and *Thread Count*, which control parallelization, also significantly affect performance. We evaluate the performance of LLMs on XR devices with varying batch sizes and thread counts to assess their processing speed, calculated using Eq. (3). The two tests conducted are described below:

- **BT:** We set PP to 64, TG to 0, and varied the batch sizes between 128, 256, 512, and 1024, with all other parameters kept at their default values.
- **TT:** We set PP to 64 and TG to 0, while varying the thread counts between 1, 2, 4, 8, 16, and 32. All other parameters were kept at their default values.

The results are shown in Section 5.4.

4.5 Evaluation of Memory Consumption

Memory consumption M_{ij} is measured in terms of the Resident Set Size (RSS) which represents the actual physical memory usage of the relevant processes. For each model-device pair (m_i, d_j) , we measure memory usage over three runs, and report the average. The memory usage for PP and TG parameters was evaluated using the same approach as the performance consistency assessment. In each test, a fixed prompt was provided, and the model was instructed to generate outputs. The experiments were conducted with batch sizes of 128, 256, 512, and 1024, and their average memory consumption was recorded. The results are shown in Section 5.5.

4.6 Battery Consumption

This section presents battery consumption rates during extended PP and TG tests. From our initial investigation, we observed that only AVP exhibited a slight impact of model size on battery consumption, while the other three devices did not show significant variations with changing model sizes. Given this observation, instead of testing all 17 models, we conducted battery tests on selected models. Specifically, we chose m_1 as the sole model from the Qwen Series. For the remaining series, we selected the smallest and largest models: m_2 and m_5 from the Vikhr-Gemma Series, m_6 and m_{11} from the Phi-3.1 Series, m_{12} and m_{13} from the LLaMA-2 Series, and m_{14} and m_{17} from the Mistral-7B Series. For each experiment, we recorded the battery level at the start and end of the experiment, allowing us to calculate battery consumption over a fixed duration of 600 seconds (10 minutes). Each experiment was repeated three times, and we reported the mean values. To ensure consistent conditions, we took a 600-second break between experiments, allowing the devices to cool down. The results are presented in Section 5.6.

4.7 Pareto Optimality

Although we evaluate our five performance metrics across various devices and models, the metrics remain fragmented and cannot be directly compared with other metrics. To address this, we turn to *Pareto efficiency* theory [30], which provides a measure of efficiency in multi-objective contexts and has been widely applied in various system design approaches [31], [32]. A choice is considered Pareto optimal if no other choice exists that can improve any of its objective criteria without deteriorating at least one other criterion. In our case, x_1 is considered dominated by x_2 through objects f if :

$$f_i(x_1) \leq f_i(x_2) \quad \forall i \in \{1, \dots, m\} \\ \text{and } \exists j \in \{1, \dots, m\} \mid f_j(x_1) < f_j(x_2) \quad (6)$$

where i, j represent different objective indices.

A choice x^* is considered Pareto optimal if no other feasible option dominates it. The set of all non-dominated designs forms the Pareto front, which represents the optimal trade-offs between all objectives.

To identify the optimal choices across devices and models, we define three objectives: *quality*, *performance*, and *stability*. To calculate the final score for each objective, we propose Eq. (7). For a given device-model pair and a specific objective, we first apply min-max normalization to each metric across all device-model pairs to eliminate the impact of different scales. Then, we

compute a weighted sum of all metrics for that pair to obtain a single score:

$$f_o(x) = \sum_{i=1}^n w_i \cdot \frac{m_i(x) - \min(m_i)}{\max(m_i) - \min(m_i)} \quad (7)$$

where o is the objective index, n is the number of metrics used in the objective category, w_i defines the weight for each metric, and min and max calculate the minimum and maximum values across the entire set of results for metric m_i .

In practice, some metrics, such as perplexity, are better when lower, which is the opposite of the direction in Eq. (6). Therefore, we take the reciprocal of each perplexity value.

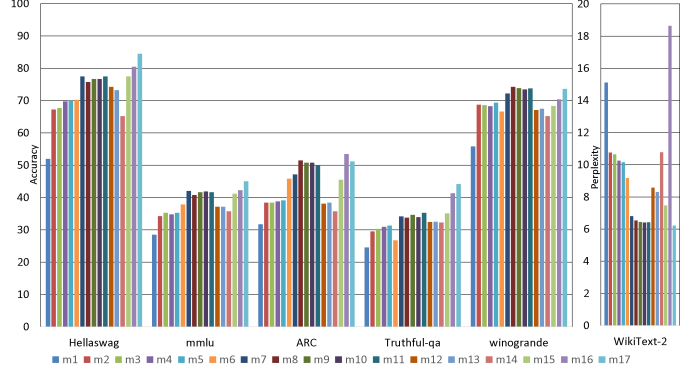


Fig. 2. Model Quality Analysis: The models were evaluated based on six different benchmarks. We chose accuracy (\uparrow) for the five benchmarks on the left and perplexity (\downarrow) for the WikiText-2 benchmark. Each group in the bar chart represents models m_1 to m_{17} from left to right.

5 PERFORMANCE EVALUATION RESULTS

This section presents the results of four types of experiments described in Section 4.

5.1 Model Quality Analysis

As shown in Table 1, we select five different model architectures, and for each architecture, we choose various quantization settings. While lower-bit quantization reduces model size, speeds up inference, and lowers power consumption, it typically comes at the cost of reduced model performance. The results of the model quality are illustrated in Fig. 2. As shown in Fig. 2, a consistent trend is observed across all benchmarks: applying lower-bit quantization settings results in reduced model performance. Models with more parameters exhibit better language understanding capabilities, leading to higher performance under the same quantization settings. Additionally, different benchmarks exhibit varying levels of sensitivity to the quantization settings. For example, Hellaswag, ARC and WikiText-2 are more sensitive compared to the other three benchmarks.

5.2 Performance Consistency Results

Figures 3 and 4 illustrate the consistency of performance across all model-device pairs, while Table 2 provides the corresponding quantitative results. Across all 20 runs, the Apple Vision Pro demonstrates the most consistent results compared to other devices, with the corresponding speed also being the fastest. Notably, the GPU results for the Apple Vision Pro exhibit greater stability

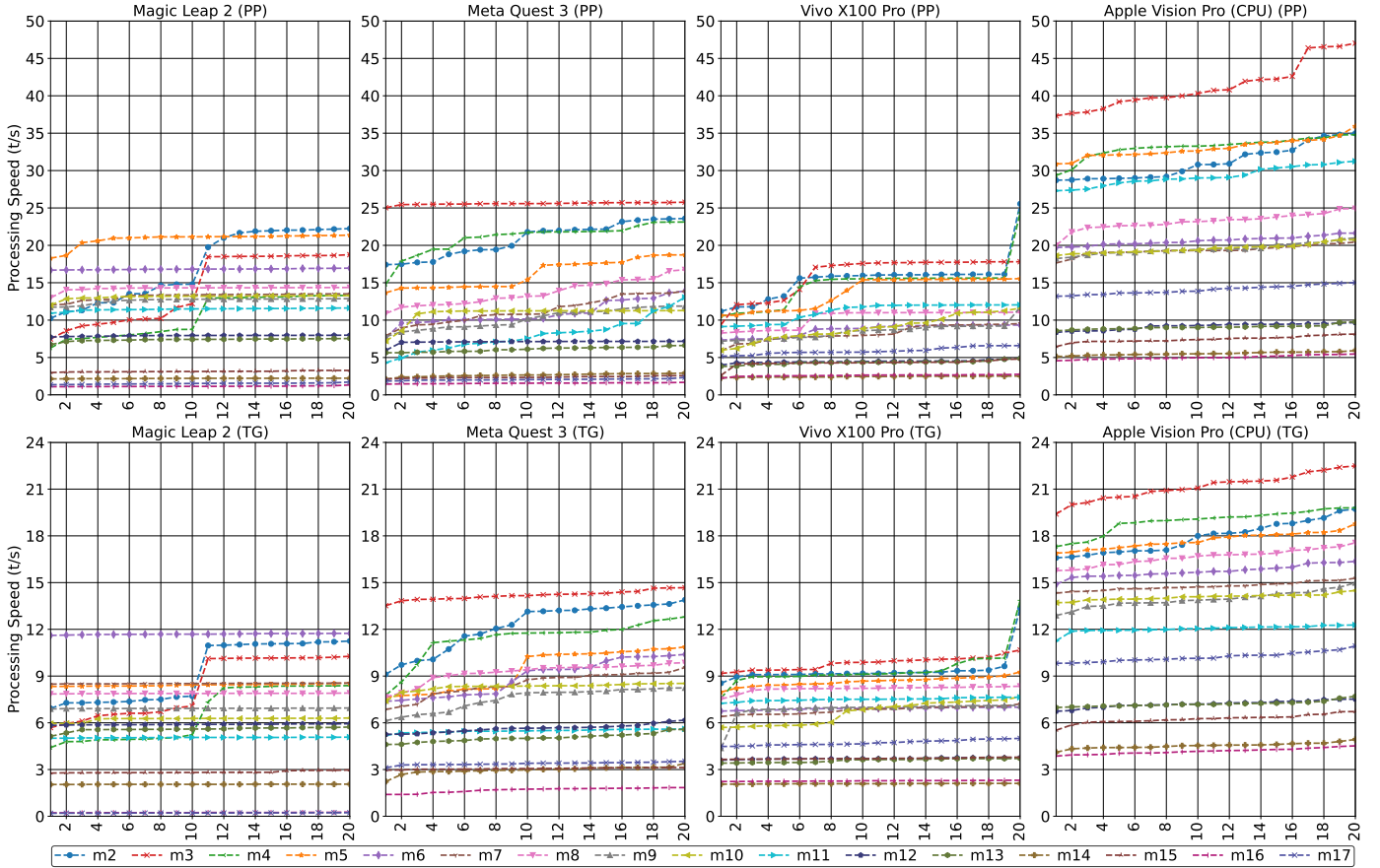


Fig. 3. Consistency results of the four devices over time: PP (top) and TG (bottom) speeds in tokens per second across 20 sorted runs (X-axis: run number, Y-axis: speed in t/s).

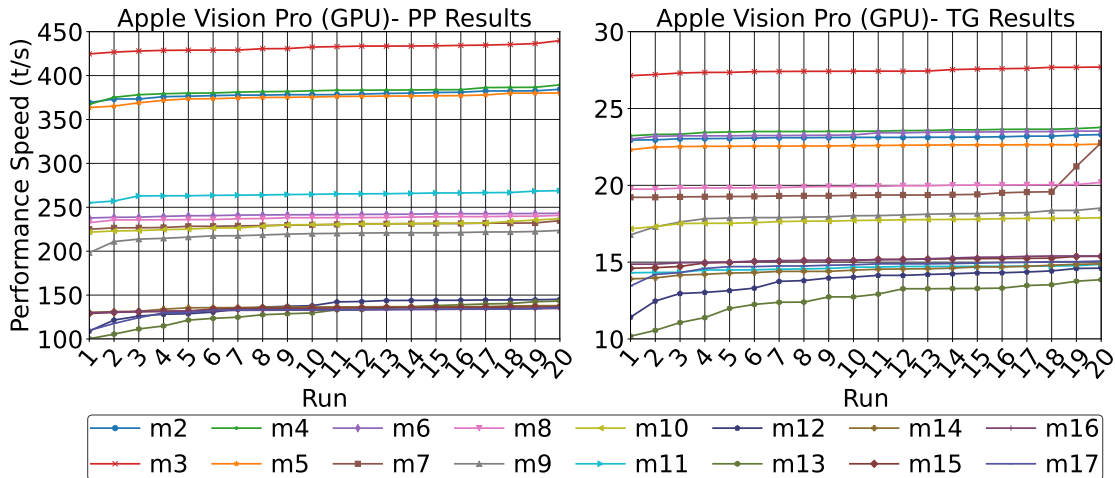


Fig. 4. Consistency results of the Apple Vision Pro on GPU. Left: PP results. Right: TG results. Each model was tested 20 times, and the results are plotted in sorted order.

and smaller variance. Among the remaining devices, the Magic Leap 2 also shows a reasonable degree of stability; however, for the first three models, its variance is surprisingly high, reaching 27%, 32%, and 26% for m_2 , m_3 , and m_3 under the PP setup, and 20%, 23%, and 27% under the TG setup, respectively. In contrast, the Meta Quest 3 and Vivo X100 Pro exhibit relatively poor performance both in terms of speed and variance. Between these two devices, the Meta Quest 3 achieves higher speeds than the Vivo X100 Pro, but there is no clear difference in variance. For some models, one device shows lower variance, while for others,

the variance is higher.

Furthermore, as shown in Table 3 performance varies significantly for m_1 over Magic Leap 2 and Meta Quest 3, but it is generally consistent across the other two devices. These findings suggest that, provided model-device pairs are carefully selected, LLM performance can be considered reliable, strengthening the case for on-device LLM use in XR environments.

TABLE 2

Performance consistency results for the four devices: Magic Leap 2 (ML2), Meta Quest 3 (MQ3), Vivo X100 Pro (Vivo), and Apple Vision Pro (VPro for CPU and VPro* for GPU). Processing speed was calculated from 20 runs for each model-device pair. The results are reported in terms of the mean (μ) speed (t/s) of 20 runs, its standard deviation (σ), coefficient of variation (CV %), and the range of values: $[min, max]$.

D	Metric	m																
		m2	m3	m4	m5	m6	m7	m8	m9	m10	m11	m12	m13	m14	m15	m16	m17	
PP Results	$\mu \pm \sigma$	17.01 ± 4.67	13.99 ± 4.57	10.38 ± 2.74	20.82 ± 0.87	16.81 ± 0.07	13.16 ± 0.47	14.22 ± 0.31	12.63 ± 0.38	13.12 ± 0.29	11.45 ± 0.18	7.92 ± 0.05	7.37 ± 0.19	2.20 ± 0.33	3.14 ± 0.08	1.15 ± 0.05	1.52 ± 0.09	
	Range	[10.25, 22.24]	[7.47, 18.75]	[6.27, 13.32]	[18.28, 21.36]	[16.68, 16.95]	[12.04, 13.51]	[12.98, 14.36]	[11.73, 12.87]	[12.00, 13.27]	[10.93, 11.62]	[7.73, 7.99]	[6.73, 7.54]	[2.14, 2.23]	[2.98, 3.27]	[1.10, 1.33]	[1.36, 1.72]	
	CV (%)	27.46	32.66	26.41	4.16	0.43	3.56	2.19	2.98	2.22	1.57	0.66	2.54	1.35	2.41	4.70	5.99	
	$\mu \pm \sigma$	21.00 ± 2.16	25.61 ± 0.10	21.33 ± 1.47	16.33 ± 1.84	10.99 ± 1.65	11.37 ± 1.80	13.74 ± 1.72	10.24 ± 1.34	11.07 ± 0.61	8.17 ± 2.19	7.12 ± 0.04	6.09 ± 0.32	2.65 ± 0.21	2.37 ± 0.12	1.57 ± 0.06	2.04 ± 0.09	
	Range	[17.42, 23.59]	[25.03, 25.77]	[14.79, 23.12]	[13.66, 18.72]	[7.62, 13.89]	[7.91, 13.86]	[10.88, 16.74]	[7.79, 11.87]	[7.19, 11.28]	[4.31, 13.05]	[5.96, 7.17]	[5.64, 6.61]	[2.10, 2.92]	[2.12, 2.57]	[1.44, 1.68]	[1.85, 2.34]	
	CV (%)	10.27	0.37	6.89	11.24	14.99	15.80	12.51	13.06	5.55	26.81	0.56	5.23	7.84	5.24	3.93	4.23	
	$\mu \pm \sigma$	15.70 ± 2.88	15.90 ± 2.76	14.98 ± 2.98	13.77 ± 2.13	8.66 ± 0.80	8.27 ± 1.08	10.35 ± 1.10	8.48 ± 1.08	8.82 ± 1.61	11.14 ± 1.21	4.47 ± 0.19	4.35 ± 0.23	2.44 ± 0.07	4.28 ± 0.44	2.61 ± 0.12	5.89 ± 0.47	
	Range	[11.16, 25.55]	[9.39, 17.81]	[10.52, 24.36]	[10.65, 15.55]	[7.32, 9.34]	[5.88, 9.53]	[8.27, 11.05]	[7.19, 11.72]	[5.97, 11.60]	[9.13, 12.04]	[3.98, 4.92]	[3.80, 4.86]	[2.27, 2.52]	[2.61, 4.80]	[2.23, 2.76]	[5.17, 6.59]	
	CV (%)	18.33	17.38	19.88	15.50	9.26	13.07	10.61	12.75	18.31	10.84	4.24	5.39	3.00	10.30	4.55	7.92	
	$\mu \pm \sigma$	31.03 ± 2.20	41.22 ± 3.04	33.11 ± 1.35	32.96 ± 1.21	20.62 ± 0.56	19.34 ± 0.64	23.14 ± 1.09	19.52 ± 0.73	19.56 ± 0.60	29.22 ± 1.22	9.15 ± 0.40	9.06 ± 0.28	5.52 ± 0.21	7.44 ± 0.40	5.01 ± 0.26	14.05 ± 0.56	
Range	[29, 34.98]	[39.44, 47.03]	[32.98, 34.79]	[32.15, 35.93]	[20.19, 21.63]	[19.09, 20.43]	[22.65, 24.92]	[19.04, 20.98]	[19.15, 20.74]	[28.58, 31.25]	[8.77, 9.67]	[8.88, 9.77]	[5.4, 5.93]	[7.21, 8.13]	[4.83, 5.47]	[13.63, 15.02]		
CV (%)	7.08	7.37	4.07	3.68	2.72	3.31	4.69	3.72	3.05	4.17	4.41	3.12	3.73	5.38	5.16	3.99		
$\mu \pm \sigma$	378 ± 3.7	432 ± 3.7	382 ± 4.8	374 ± 4.6	241 ± 1.5	230 ± 2.3	237 ± 2.0	218 ± 5.8	229 ± 4.3	264 ± 3.4	136 ± 9.9	128 ± 12.5	135 ± 2.3	134 ± 2.3	133 ± 1.4	130 ± 6.6		
Range	[369, 384]	[424, 439]	[367, 389]	[363, 380]	[237, 243]	[225, 234]	[232, 240]	[198, 223]	[221, 237]	[255, 268]	[109, 145]	[100, 143]	[130, 138]	[129, 136]	[129, 134]	[109, 135]		
CV (%)	1.0	0.9	1.2	1.2	0.6	1.0	0.8	2.6	1.9	1.3	7.3	9.8	1.7	1.7	1.1	5.1		
TG Results	$\mu \pm \sigma$	9.14 ± 1.92	8.22 ± 1.92	6.53 ± 1.77	8.43 ± 0.07	11.69 ± 0.04	8.52 ± 0.02	7.88 ± 0.01	6.92 ± 0.01	6.25 ± 0.10	5.05 ± 0.02	5.90 ± 0.03	5.59 ± 0.14	2.05 ± 0.21	2.84 ± 0.06	0.24 ± 0.01	0.21 ± 0.01	
	Range	[6.92, 11.25]	[5.69, 10.27]	[4.41, 8.39]	[8.33, 8.55]	[11.61, 11.74]	[8.48, 8.55]	[7.85, 7.91]	[6.89, 6.95]	[5.95, 6.31]	[5.01, 5.08]	[5.83, 5.94]	[5.13, 5.73]	[2.04, 2.06]	[2.77, 2.97]	[0.22, 0.27]	[0.19, 0.23]	
	CV (%)	20.95	23.36	27.10	0.77	0.32	0.23	0.18	0.21	1.62	0.39	0.48	2.49	0.32	2.24	5.32	5.20	
	$\mu \pm \sigma$	12.37 ± 1.45	14.19 ± 0.30	11.58 ± 0.98	9.47 ± 1.29	9.00 ± 1.12	8.57 ± 0.70	9.30 ± 0.51	7.61 ± 0.65	8.30 ± 0.26	5.47 ± 0.10	5.62 ± 0.23	5.01 ± 0.24	2.95 ± 0.21	3.06 ± 0.05	1.67 ± 0.15	3.38 ± 0.09	
	Range	[9.11, 13.89]	[13.52, 14.67]	[7.77, 12.80]	[7.64, 10.87]	[7.38, 10.39]	[6.85, 9.55]	[7.66, 9.86]	[6.13, 8.24]	[7.40, 8.53]	[5.19, 5.61]	[5.26, 6.17]	[4.61, 5.57]	[2.23, 3.40]	[2.96, 3.13]	[1.40, 1.84]	[3.11, 3.53]	
	CV (%)	11.73	2.11	8.43	13.65	12.50	8.17	5.52	8.51	3.18	1.87	4.09	4.83	7.27	1.68	8.93	2.80	
	$\mu \pm \sigma$	9.39 ± 0.98	9.85 ± 0.42	9.44 ± 1.22	8.66 ± 0.30	6.91 ± 0.08	6.83 ± 0.22	8.21 ± 0.12	6.84 ± 0.61	6.61 ± 0.71	7.51 ± 0.11	3.70 ± 0.53	5.59 ± 0.11	2.09 ± 0.01	3.71 ± 0.04	2.27 ± 0.02	4.72 ± 0.17	
	Range	[8.54, 13.35]	[9.17, 10.67]	[7.58, 13.86]	[7.97, 9.26]	[6.75, 7.00]	[6.39, 7.21]	[7.52, 8.35]	[4.37, 7.11]	[5.70, 7.68]	[7.25, 7.64]	[3.60, 3.77]	[3.41, 3.71]	[2.06, 2.11]	[3.65, 3.79]	[2.23, 2.31]	[4.48, 5.00]	
	CV (%)	10.46	4.22	12.91	3.48	1.13	3.25	1.48	8.92	10.75	1.41	1.27	3.04	0.68	1.15	1.06	3.61	
	$\mu \pm \sigma$	17.90 ± 1.00	21.15 ± 0.82	18.92 ± 0.74	17.71 ± 0.50	15.72 ± 0.37	14.76 ± 0.26	16.63 ± 0.49	13.93 ± 0.50	14.07 ± 0.19	12.03 ± 0.21	7.20 ± 0.21	7.22 ± 0.17	4.53 ± 0.17	6.24 ± 0.27	4.17 ± 0.18	10.22 ± 0.30	
Range	[16.59, 19.72]	[19.4, 22.49]	[17.31, 19.8]	[16.89, 18.77]	[14.88, 16.36]	[14.32, 15.28]	[15.77, 17.56]	[12.89, 14.99]	[13.71, 14.49]	[11.26, 12.28]	[6.74, 7.52]	[6.98, 7.7]	[4.11, 4.93]	[5.52, 6.72]	[3.86, 4.52]	[9.82, 10.93]		
CV (%)	5.58	3.86	3.89	2.84	2.35	1.73	2.97	3.61	1.35	1.77	2.95	2.41	3.84	4.35	4.31	2.91		
$\mu \pm \sigma$	23.1 ± 0.1	27.5 ± 0.1	23.5 ± 0.1	22.6 ± 0.1	23.3 ± 0.1	19.6 ± 0.8	19.9 ± 0.1	18.0 ± 0.4	17.7 ± 0.2	14.6 ± 0.2	13.7 ± 0.8	12.5 ± 1.0	14.5 ± 0.3	15.1 ± 0.2	15.2 ± 0.2	14.7 ± 0.4		
Range	[23, 23.3]	[27.1, 27.7]	[23.2, 23.8]	[22.3, 22.7]	[23.0, 23.5]	[19.2, 22.8]	[19.8, 20.2]	[16.8, 18.5]	[17.2, 17.9]	[14.3, 14.9]	[11.4, 14.6]	[10.2, 13.9]	[13.9, 14.9]	[14.6, 15.4]	[14.9, 15.4]	[13.5, 15.1]		
CV (%)	0.4	0.5	0.5	0.3	0.6	4.3	0.6	2.1	1.0	1.1	5.8	8.3	1.9	1.4	1.1	2.5		

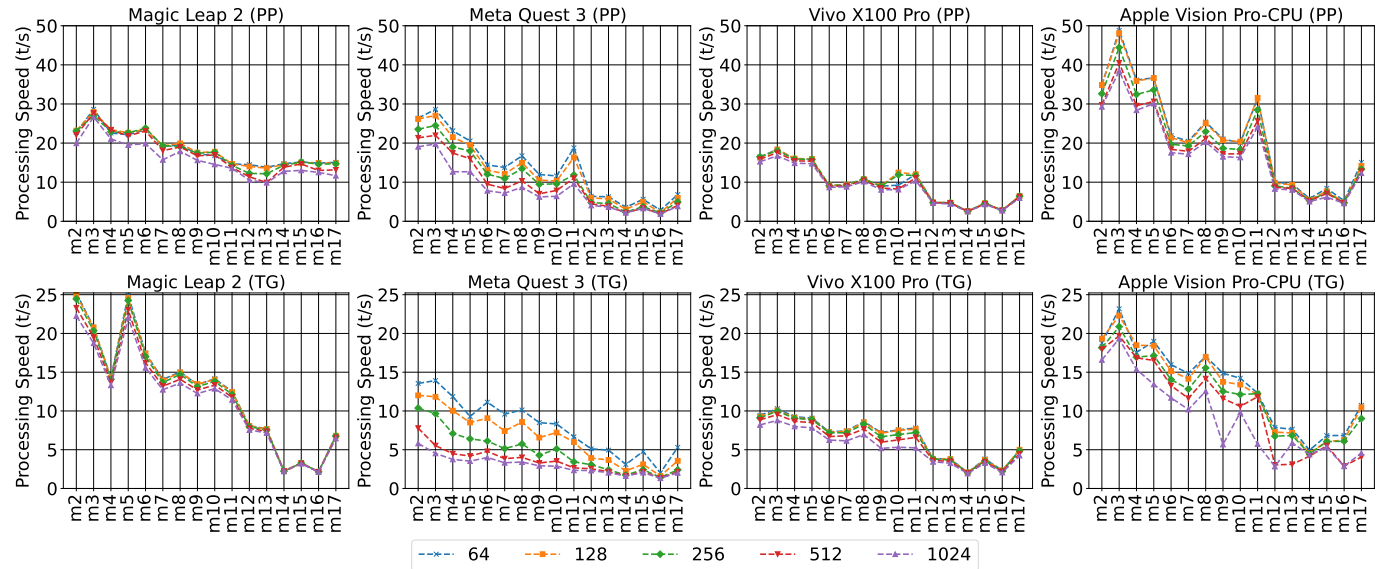


Fig. 5. Processing speed of the four devices in the PP test (top) and TG test (bottom) with varying string lengths: 64, 128, 256, 512, and 1024. The x-axis represents the model, while the y-axis represents the processing speed in t/s.

TABLE 3

Performance consistency results for m_1 across the four devices. For the results of other models and description of metrics used, see Table 2.

Test	Metric	ML2	Vivo	Meta Q3	VisPro	VisPro*
PP	$\mu \pm \sigma$	51.68 ± 4.22	62.68 ± 16.64	39.32 ± 15.66	292.48 ± 12.87	1603.59 ± 56.12
	Range	[43.62, 54.59]	[21.63, 72.04]	[24.25, 72.59]	[288.5, 312.1]	[1516.9, 1696.1]
	CV (%)	8.17	26.55	39.82	4.40	3.50
TG	$\mu \pm \sigma$	20.26 ± 0.05	22.16 ± 0.90	16.76 ± 3.76	41.94 ± 1.77	42.94 ± 0.80
	Range	[20.17, 20.34]	[20.54, 23.41]	[11.61, 22.53]	[38.90, 46.37]	[41.76, 44.35]
	CV (%)	0.23	4.05	22.44	4.21	1.87

5.3 Results of Processing Speed and String Length

Figs. 5 and 6 present the processing speed results of PP and TG with varying string lengths (prompt length and token sets). Both PP and TG were tested with values of 64, 128, 256, 512, and 1024. The processing speed varies significantly across string lengths, devices, and models.

String length and PP vs TG Speed: PP speed is consistently

higher than TG speed, with a speedup of approximately two to three times across the four (CPU-based) devices, while on

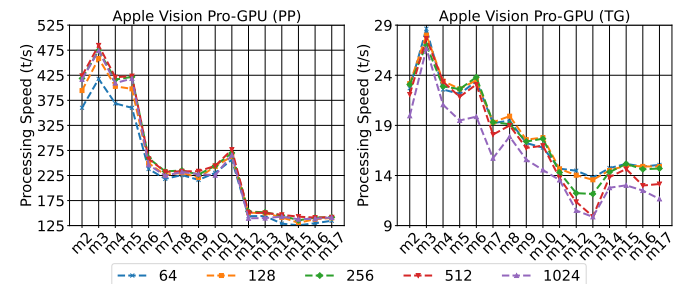


Fig. 6. Processing speed of Apple Vision Pro (GPU) in the PP test (left) and TG test (right). The x-axis represents the model, while the y-axis represents the processing speed in t/s.

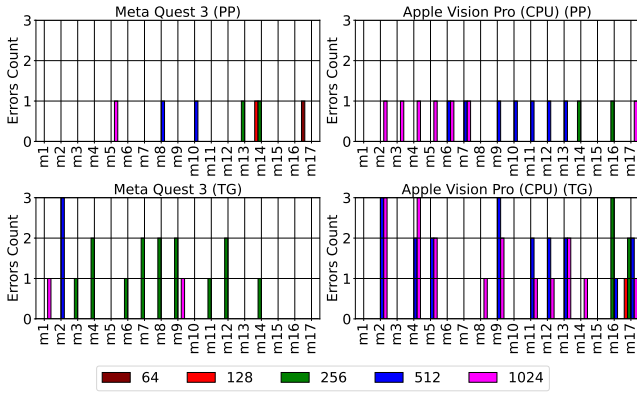


Fig. 7. Error counts for Meta Quest 3 (left) and Apple Vision Pro (right) in PP (top) and TG (bottom). Magic Leap 2, with zero errors, and Vivo X100 Pro, with a total of four errors, one in m_1 (PP-64), two in m_{10} (PP-64, PP-128), and one in m_{11} (TG-1024) are excluded.

AVP (GPU), the PP speed is significantly higher, ranging from 10 to 19 times the TG speed. Similarly, increasing the prompt size slightly reduces the prompt processing speed in PP, whereas in TG, the speed reduction is more significant with a growing token set. This suggests that TG has a higher computational cost due to its sequential execution of tokens, whereas PP is somewhat parallelized, requiring only the loading of prompts. Though there is minor variation in the 64, 128, and 256 string lengths, the last two, 512 and 1024, are consistently the slowest. When examining the variation across string lengths, MQ3 exhibits the largest variance, whereas ML2 and AVP have the smallest variance.

Device-Based Analysis: If we examine the devices, the overall performance trends reveal that AVP consistently shows the highest speed in both PP and TG tests. ML2 ranks second in both PP and TG performance, while Vivo X100s Pro outperforms MQ3 in TG (particularly in longer strings 512, 1024) but ranks fourth in PP. This ranking highlights the varying computational capabilities of XR devices, with AVP (both CPU and GPU) standing out as the fastest one across all conditions. ML2 shows stable performance across all variations of string lengths, with lower $CV\%$ values, indicating that it does not vary significantly with changing string lengths. In contrast, MQ3 shows a higher $CV\%$, indicating greater variance with increasing string length.

Error Counts: Figure 7 shows the errors counts during the PP and TG tests. Errors mostly occurred in AVP (CPU) and MQ3, particularly at longer prompt lengths of 512 and 1024 tokens. There are a few reasons for this. First, longer strings process more slowly, leading to abrupt changes and occasional failures. Second, memory constraints or inefficiencies in sustained generation contribute to these errors. With AVP, the general user experience is also suboptimal, as the device must be actively mounted on the head, which can cause errors if not handled carefully. Overall, MQ3 records the highest count of errors, with frequent retries affecting its reliability, whereas ML2 remains highly stable, leading to minimal inconsistencies (zero errors). As expected, AVP (GPU) also reported zero errors.

Model-Based Analysis: In the model-wise analysis, smaller models such as Qwen2-0.5B and Vikhr-Gemma-2B achieve the highest speeds across devices, particularly in PP. In contrast, larger models like the LLaMA-2-7B series and Mistral-7B series exhibit significantly lower processing speeds, with higher variability and

instability, especially in TG. Model size also impacts processing speed, as smaller models are faster. Here, m_1 is the fastest (though omitted from later analysis), while m_2 , m_3 , and m_5 are the fastest among the remaining models, whereas m_{14} and m_{16} are the slowest.

5.4 Results of Parallelization with BT and TT

This section presents the results of BT and TT, both of which are used to achieve concurrency and parallelization. Regardless of the parallelization method, the three models m_2 , m_3 , and m_5 consistently rank among the fastest across all devices, while m_{14} and m_{16} are the slowest.

Results of BT: Fig. 8 presents the results of the batch test with varying batch sizes of 128, 256, 512, and 1024. Generally, increasing the batch size leads to a decrease in performance across all four devices (except for AVP (GPU)) due to increased computational overhead. AVP (GPU), with its strong computational resources, does not show a significant performance drop with varying batch sizes, although there are some fluctuations at a batch size of 256. This indicates that GPU-based processing on AVP (GPU) is highly optimized for parallel execution and can effectively manage larger batches of input without affecting processing speed.

More importantly, AVP (CPU) experiences a noticeable performance drop as the batch size increases. However, the remaining devices do not follow this trend. For instance, on MQ3, batch size 128 yields the best performance, whereas for the other batch sizes, there is no significant change. Similarly, for ML2 and Vivo, variations in batch size do not appear to have a substantial impact on performance.

Results of TT: Fig. 9 presents the TT results for thread counts of 1, 2, 4, 8, 16, and 32. Across all four devices, processing speed sees the most significant increase when increasing the thread count from 1 to 4. The speed gain continues at 8 threads (or shows minor degradation), but beyond 8 threads, performance begins to decline slightly, with further degradation beyond 16 threads. Apple Vision Pro (CPU) fails at thread counts of 16 and 32, indicating its limitations in achieving this level of parallelism.

AVP (GPU) follows a different trend, maintaining consistently high processing speed across all thread counts. Unlike CPU-based devices, its performance remains stable even at 32 threads, demonstrating its superior ability to handle concurrent tasks. These results highlight that while the four CPU-based devices benefit from moderate threading, AVP (GPU) is significantly more efficient at scaling concurrency without experiencing notable performance degradation. Since our study primarily focuses on CPU-based implementation, we conclude that using a moderate thread count of 4, 6, or 8 yields optimal results.

5.5 Memory Consumption Results

Fig. 10 presents the memory consumption results for each model-device pair. The values represent the mean memory consumption from five experiments with varying batch sizes of 128, 256, 512, and 1024. As expected, memory consumption varies across models, with most showing consistent usage across different devices. Generally, within each model series, memory consumption increases with model size. However, minor exceptions exist, such as m_7 on Apple Vision Pro (GPU), which consumes more memory than other models in the Phi-3.1 series [$m_6 - m_{11}$]. This size-based trend does not necessarily hold across series, even for models of similar sizes. For example, m_2 (1.36 GB) consumes less memory

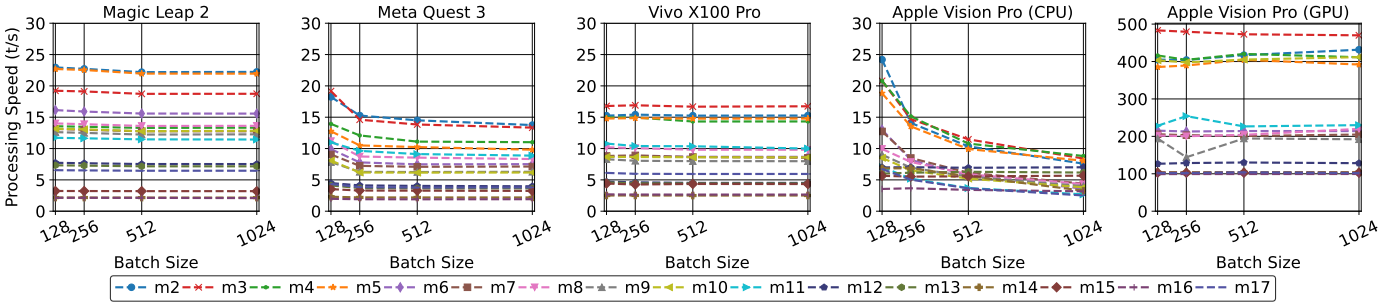


Fig. 8. Batch Test results: Batch size (X-axis) vs. processing speed (Y-axis).

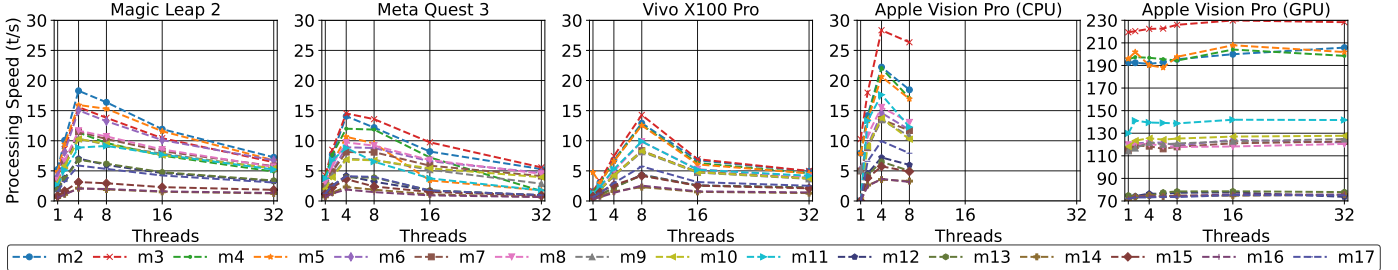


Fig. 9. Thread Test (TT) results: The X-axis represents the thread count, while the Y-axis shows the speed in tokens per second. Threads 4 and 8 deliver the fastest results. Note: Apple Vision Pro (CPU) fails for thread counts of 16 and 32.

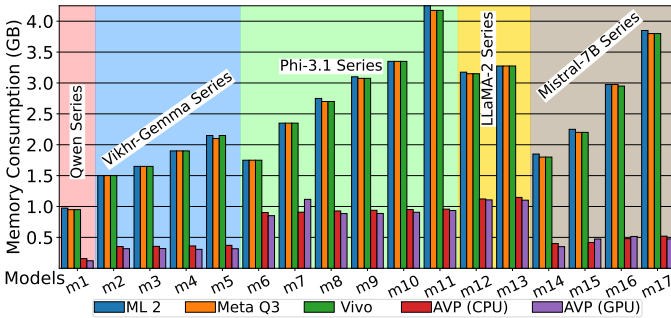


Fig. 10. Memory consumption for each model-device pair. The results represent the mean values across batch sizes 128, 256, 512, and 1024.

than m_6 (1.32 GB) despite having a larger size, as they belong to different series. Similarly, m_7 (1.94 GB) requires more memory than m_5 (2.0 GB) and m_{15} (2.05 GB), as all three belong to different series. Another example is m_{12} (2.63 GB) consuming more memory than m_{16} (2.81 GB), despite being smaller in size. From a device-specific perspective, Apple Vision Pro demonstrates significantly lower memory consumption than the other devices, averaging 0.5782 GB on the CPU and 0.5488 GB on the GPU across all 17 models. Among the remaining devices, Meta Quest 3 consumes the least memory at 2.3520 GB, followed by Vivo X100 Pro at 2.3540 GB, while Magic Leap 2 exhibits the highest at 2.3748 GB. These findings suggest that Apple Vision Pro (both CPU and GPU) is approximately four times more memory-efficient than Magic Leap 2, Meta Quest 3, and Vivo X100 Pro. Its superior memory management and hardware optimizations make it the most efficient device in terms of memory consumption.

5.6 Battery Consumption Results

Figure 11 presents the battery consumption results over a 10-minute experiment. We observe that for the first two series, the Qwen Series and Vikhr-Gemma Series, battery consumption remains relatively low and with lower variation across all four

devices. However, for larger models in the LLaMA-2 Series and Mistral-7B Series, battery consumption increases significantly. AVP shows a strong correlation between model size and battery consumption, both for GPU and CPU usage. In contrast, the remaining three devices do not exhibit a significant variation with respect to model size. Vivo demonstrates the best battery life, with an average loss of only 2.5% over 10 minutes. ML2 follows with a 8.5% average battery loss, while MQ3 records a slightly higher battery loss at 9.7%. AVP shows the worst in this regard, with GPU usage resulting in a 10.1% battery loss and with CPU usage leading to a 12.6% battery loss in 10 minutes.

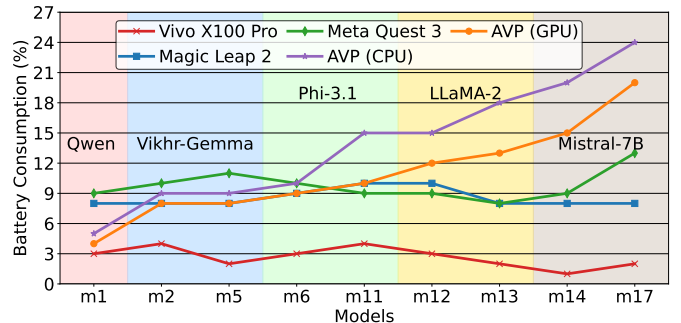


Fig. 11. Battery Consumption in 10-minute experiments.

5.7 Pareto Front Results

Since we use both CPU and GPU for inference in the Vision Pro experiments, while the other three devices use CPU only for inference, we exclude Apple Vision Pro GPU from the Pareto calculation to ensure a fair comparison. With 4 devices and 16 models (m_2 - m_{17}), we have a total of 64 device-model pairs. Using Eq. (6) and Eq. (7), we calculated the *quality*, *stability* and *performance* scores for each pair, then identified the Pareto fronts and visualized them in Fig. 12. The quality of a model can be evaluated using various benchmarks, such as accuracy and perplexity, as detailed in Section 4.1. For the performance objective,

we evaluate performance using *PP*, *TG*, *memory consumption*, and *battery consumption*, with respective weights of 0.35, 0.35, 0.2, and 0.1. For the stability objective, we assess it based on the coefficient of variation (*CV*) and error count of *PP* and *TG*, assigning 0.7 to *CV* and 0.3 to error count.

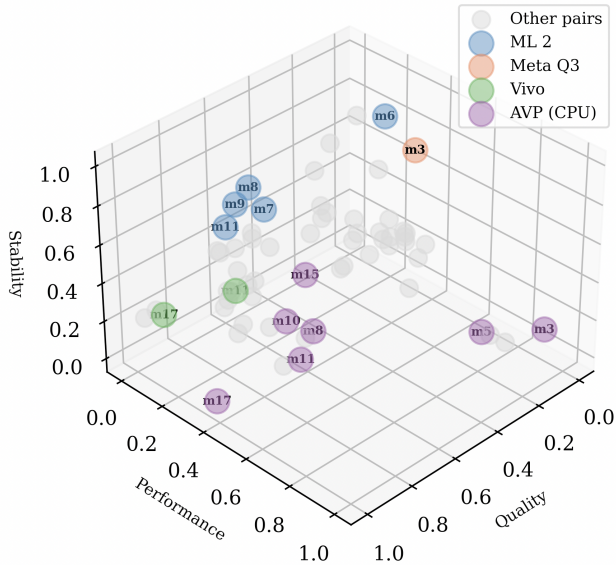


Fig. 12. Pareto fronts for various device-model pairs, with different colors representing distinct device types. Performance is evaluated based on processing speed, memory consumption, and battery consumption. Stability is assessed using the *CV* and *error count* values of *PP* and *TG*. Quality is measured through evaluation results on six benchmark datasets.

Figure 12 illustrates the Pareto front points, highlighting the optimal choices across different model sizes and devices. For example, the AVP (CPU) device achieves the highest speed among the models but exhibits relatively low stability, whereas the ML 2 device offers the greatest stability. Meanwhile, both Vivo and Meta Q3 deliver a balanced trade-off between speed and stability. At the model-pair level, m_{17} and m_{11} provide high quality on AVP (CPU) and Vivo, respectively. At the same time, m_3 is selected as a Pareto-optimal choice due to its high performance on AVP (CPU) and robust stability on Meta Q3. A similar trend is observed with m_8 , which attains strong performance and quality on AVP (CPU) as well as commendable quality and stability on ML 2.

6 DISCUSSION

We have performed extensive testing of multiple open-source language models on four distinct devices, ranging from the two-year-old Magic Leap 2, representing the state of the art in passive see-through AR devices, to Meta Quest 3, arguably the most common VR headset worldwide, and VIVO X100s Pro as an indication of the performance of next-generation mobile computing, up to Apple Vision Pro, the highest-performance VR headset on the market. The performance in all devices shows that each of the devices currently available on the market is capable of LLM inference, achieving several tokens per second, and each of them can be used as an autonomous device for performing LLM inference for a given task.

The deployment of LLMs was achieved through a customized implementation of the *Llama* [22] library for each device. We selected *Llama* due to its C++-based architecture, which offers portability, flexibility, and seamless integration across various

platforms and applications. This customization enables *Llama* to perform core LLMs tasks such as *PP* and *TG*, while providing the flexibility to adjust control parameters such as string length, batch size, and thread counts.

Our study identifies critical performance evaluation factors and introduces a suite of testing scripts to analyze these aspects systematically. These scripts enhance the reproducibility of our findings, making them relevant for future analyses in similar contexts. The processing speed, measured in tokens per second, was evaluated across multiple dimensions. This includes a consistency analysis to determine whether each model-device pair maintains stable performance over time or exhibits fluctuations. The impact of string length on both *PP* and *TG* was analyzed for each model-device combination. Additionally, the study examined the support for parallelization and concurrency control through *BT* and *TT* tests. Furthermore, memory usage and battery consumption were also assessed to provide a holistic evaluation of system performance.

For consistency analysis, we ran each model-device pair 20 times with conservative time intervals to observe performance variations. We reported the lowest and highest speeds, mean speed, standard deviation, and coefficient of variance (*CV*). Examining Figs. 3 and 4, which present the results in ascending order, we observe that the AVP GPU exhibits the highest stability. Among CPU-based devices, the AVP CPU and ML2 demonstrate the most stable performance. The quantitative results, particularly the *CV* values reported in Tables 2 and 3, further reinforce this observation. While ML2 shows a similar level of stability to the AVP CPU, its first three models (m_2 , m_3 , and m_4) exhibit a *CV* above 20% for *TG* and above 26% for *PP*. Considering the error count in Fig. 7, ML2 emerges as the most stable device, having recorded zero errors. In contrast, the AVP CPU encountered multiple errors. The remaining two devices, Vivo and MQ3, exhibit higher instability, with Vivo performing relatively better than MQ3. This also indicates that consistency is model-dependent, as seen with models m_2 , m_3 , and m_4 , which exhibited reduced stability.

For m_1 , being the smallest model, all devices performed efficiently. Among the remaining models (m_2 to m_{16}), the average inference speeds across various devices are as follows. AVP (CPU) achieved the highest inference speed (16.91 t/s *PP*, 11.04 t/s *TG*), followed by ML2 (12.68 t/s *PP*, 8.51 t/s *TG*), MQ3 (9.52 t/s *PP*, 5.77 t/s *TG*), and Vivo (8.62 t/s *PP*, 6.12 t/s *TG*), reflecting performance variations across XR devices. These speeds meet basic conversational requirements and enable LLM inference for broader applications beyond dialogue-based tasks. The *PP* speed across all devices is two to three times faster than *TG* speed, while for AVP GPU *PP* speed is 10 to 19 times faster than *TG* speed. This is because *PP* only encodes the input, whereas *TG* must process sequential dependencies during decoding. In model-based analysis, smaller models such as m_1 , m_2 , m_3 , and m_5 are the fastest, while m_{14} and m_{16} were the slowest. Regarding string length, larger *PP* and *TG* inputs (512, 1024) are slower than shorter ones (64, 128, 256). Moreover, longer strings (512, 1024) frequently result in errors. Among devices, MQ3 exhibited the highest number of errors, followed by the AVP CPU and then Vivo. In contrast, ML2 and the AVP GPU did not experience any significant errors or inconsistencies.

In batch tests (*BT*), performance generally decreases as batch size increases across all devices, except for the AVP GPU, which remains stable regardless of batch size. The AVP CPU, however,

experiences a strong performance degradation as batch size increases, more pronounced than in other devices. For thread tests (TT), across all four devices, mid-range thread counts (4 to 8) yielded the best performance, while lower (1, 2) and higher (16, 32) thread counts resulted in lower performance. Notably, the AVP CPU fails at thread counts of 16 and 32, whereas the AVP GPU exhibits its best performance at these higher thread counts.

In terms of memory consumption, significant variations were observed across different models. Generally, larger models consumed more memory. Interestingly, each of the five model series displayed distinct memory consumption trends. Some smaller models from one series consumed more memory than larger models from another series. For instance, m_2 (with size 1.36 GB) consumes less memory than m_6 (with size 1.32 GB), highlighting the model-dependent nature of memory consumption (see Fig. 10).

Battery consumption did not show significant differences across devices, although the Apple Vision Pro exhibited slightly higher battery life loss, with an average battery depletion of up to 10.1% (with GPU) and 12.6% (with CPU) over 10 minutes. In contrast, the Vivo X100 Pro performed the best, with only a 2.5% loss, while the Magic Leap 2 demonstrated good battery efficiency with an 8.5% loss. The Meta Quest 3 consumed an average of 9.7% over the same duration.

With 3D Pareto Optimality, we found AVP leading overall, ML2 demonstrating high consistency and stability, Vivo being slower but still consistent in performance, and MQ3 ranking lowest across all aspects. Among the models, m_3 , and m_5 performed particularly well, with smaller models generally exhibiting better results. In contrast, models from the LLaMA-2 and Mistral-7B series were the slowest. Our study highlights the trade-offs between model complexity and system responsiveness. Larger models exhibit lower speed though they may offer greater accuracy and richer contextual responses. These larger models also drain batteries faster and decrease thermal stability. Conversely, lighter models enhance efficiency but may compromise response quality.

At this point, we can conclude that nowadays, the generation of XR devices is capable of executing interactive conversational tasks directly on the device. This is an important step towards XR device autonomy (and for edge devices in general) and an opportunity to perform complex tasks without any network connectivity requirement. We can anticipate that the next generation of XR devices with better computational capabilities, memory capacity, and battery life, will allow for complex on-device multimodal inference tasks, aiding users in a broad spectrum of tasks.

Limitations: Apart from the AVP, our study primarily focuses on CPU-based evaluation and does not fully explore the potential of GPU- and NPU-accelerated inference for on-device LLM deployment. The limited VRAM on the three devices (ML2, Vivo, and MQ3) restricted full model loading, which hindered GPU performance. Additionally, the specialized frameworks and configurations required for GPU and NPU optimization were beyond the scope of this work. Finally, since the study is primarily based on *Llama.cpp* implementations, its generalizability is limited.

Future Research: In future research, we plan to conduct an in-depth exploration of GPU and NPU-based deployment, aiming to optimize performance for lower-memory GPUs while maximizing efficiency. Furthermore, the integration of visual language models (VLMs) capable of processing images and graphical inputs will be ideally suited for the XR domain, expanding potential applications across various fields, including education, healthcare, and robotics. Additionally, voice- or text-based interaction with on-device

LLMs can lead to several XR applications. For example, training the voice system with a specific teacher’s voice and utilizing it as a communication medium for a teacher’s virtual avatar could create a compelling educational tool—a virtual tutor. A similar approach could also be applied to humanoid robots (or avatars in VR), enabling more natural and interactive communication.

7 CONCLUSION

LoXR presents a comprehensive study on deploying LLMs on four XR devices, conducting an in-depth analysis of multiple performance factors. Given the GPU memory limitations of most XR devices, our study primarily focuses on CPU-based analysis. However, since the AVP has sufficient GPU resources, we also include GPU results for AVP, providing additional insights into the study. Generally, for processing speed, we can rank the four devices in the following order: AVP, ML2, Vivo, and MQ3, although MQ3 outperforms Vivo in TG.

In memory consumption, AVP was found the most memory-efficient. Among the remaining devices, differences were minimal, though ML2 occasionally consumed the most memory. As expected, larger models required more memory, but this trend varied across different model series. For BT tests, a lower batch size (128) yielded the best performance, while larger batch sizes reduced speed for CPU-based tests, with AVP GPU remaining largely unaffected. For TT tests, medium thread counts (4–8) were optimal across all devices. In terms of consistency, ML2 is the most stable, exhibiting the lowest variance in speed and zero errors. AVP GPU also maintains low variance. MQ3 performs the worst in this aspect, while Vivo is more stable than MQ3 but less consistent than the rest.

The Pareto analysis highlighted several models on AVP due to their outstanding performance, while the Pareto fronts found on ML2 because of their consistently stable results. Additionally, a few models on Vivo and MQ3 emerged on the Pareto front because of their balanced trade-offs between performance and stability. Models m_{12} to m_{17} were significantly slower.

REFERENCES

- [1] T. Wu, S. He, J. Liu, S. Sun, K. Liu, Q.-L. Han, and Y. Tang, “A brief overview of ChatGPT: The history, status quo and potential future development,” *IEEE/CAA Journal of Automatica Sinica*, vol. 10, no. 5, pp. 1122–1136, 2023.
- [2] K. Eker, M. K. Pehlivanoğlu, A. G. Eker, M. A. Syakura, and N. Duru, “A comparison of grammatical error correction models in english writing,” in *2023 8th International Conference on Computer Science and Engineering (UBMK)*, 2023, pp. 218–223.
- [3] I. Adeshola and A. P. Adepoju, “The opportunities and challenges of chatgpt in education,” *Interactive Learning Environments*, vol. 0, no. 0, pp. 1–14, 2023. [Online]. Available: <https://doi.org/10.1080/10494820.2023.2253858>
- [4] Y. Feng, S. Vanam, M. Cherukupally, W. Zheng, M. Qiu, and H. Chen, “Investigating code generation performance of chatgpt with crowdsourcing social data,” in *2023 IEEE 47th Annual Computers, Software, and Applications Conference (COMPSAC)*, 2023, pp. 876–885.
- [5] S. Koch, N. Vaskevicius, M. Colosi, P. Hermosilla, and T. Ropinski, “Open3dsng: Open-vocabulary 3d scene graphs from point clouds with queryable objects and open-set relationships,” in *Proceedings of the IEEE/CVF Conference on Computer Vision and Pattern Recognition (CVPR)*, 2024, pp. 14 183–14 193.
- [6] D. Jia, A. Irger, L. Besancon, O. Strnad, D. Luo, J. Bjorklund, A. Ynnerman, and I. Viola, “Voice: Visual oracle for interaction, conversation, and explanation,” 2024.
- [7] D. Jia, Y. Wang, and I. Viola, “Chat modeling: Natural language-based procedural modeling of biological structures without training,” 2024.

- [8] Z. Liu, C. Zhao, F. Iandola, C. Lai, Y. Tian, I. Fedorov, Y. Xiong, E. Chang, Y. Shi, R. Krishnamoorthi, L. Lai, and V. Chandra, "MobileLLM: Optimizing sub-billion parameter language models for on-device use cases," in *Proceedings of ICML*, 2024, pp. 32 431–32 454.
- [9] F. De La Torre, C. M. Fang, H. Huang, A. Banburski-Fahey, J. Amores Fernandez, and J. Lanier, "LLMR: Real-time prompting of interactive worlds using large language models," in *Proc. of the CHI Conference on Human Factors in Computing Systems*, 2024, pp. 1–22.
- [10] R. Kurai, T. Hiraki, Y. Hiroi, Y. Hirao, M. Perusquia-Hernandez, H. Uchiyama, and K. Kiyokawa, "Magicitem: Dynamic behavior design of virtual objects with large language models in a consumer metaverse platform," *arXiv preprint arXiv:2406.13242*, 2024.
- [11] Y. Zhang, P. Gao, F. Kang, J. Li, J. Liu, Q. Lu, and Y. Xu, "Odoragent: Generate odor sequences for movies based on large language model," in *2024 IEEE Conference Virtual Reality and 3D User Interfaces (VR)*. IEEE, 2024, pp. 105–114.
- [12] Z. Yin, Y. Wang, T. Papatheodorou, and P. Hui, "Text2vrscene: Exploring the framework of automated text-driven generation system for vr experience," in *2024 IEEE Conference Virtual Reality and 3D User Interfaces (VR)*. IEEE, 2024, pp. 701–711.
- [13] L. Chen, Y. Cai, R. Wang, S. Ding, Y. Tang, P. Hansen, and L. Sun, "Supporting text entry in virtual reality with large language models," in *2024 IEEE Conference Virtual Reality and 3D User Interfaces (VR)*. IEEE, 2024, pp. 524–534.
- [14] D. Giunchi, N. Numan, E. Gatti, and A. Steed, "Dreamcodevr: Towards democratizing behavior design in virtual reality with speech-driven programming," in *2024 IEEE Conference Virtual Reality and 3D User Interfaces (VR)*. IEEE, 2024, pp. 579–589.
- [15] H. Wan, J. Zhang, A. A. Suria, B. Yao, D. Wang, Y. Coody, and M. Prpa, "Building llm-based ai agents in social virtual reality," in *Extended Abstracts of the CHI Conference on Human Factors in Computing Systems*, 2024, pp. 1–7.
- [16] G. Qu, Q. Chen, W. Wei, Z. Lin, X. Chen, and K. Huang, "Mobile edge intelligence for large language models: A contemporary survey," *arXiv preprint arXiv:2407.18921*, 2024.
- [17] W. Cheng, W. Zhang, H. Shen, Y. Cai, X. He, K. Lv, and Y. Liu, "Optimize weight rounding via signed gradient descent for the quantization of llms," *arXiv preprint arXiv:2309.05516*, 2023.
- [18] X. Ma, G. Fang, and X. Wang, "Llm-pruner: On the structural pruning of large language models," *Advances in neural information processing systems*, vol. 36, pp. 21 702–21 720, 2023.
- [19] Y. Gu, L. Dong, F. Wei, and M. Huang, "Minillm: Knowledge distillation of large language models," in *The Twelfth International Conference on Learning Representations*, 2024.
- [20] Z. Liu, J. Yuan, H. Jin, S. Zhong, Z. Xu, V. Braverman, B. Chen, and X. Hu, "Kivi: A tuning-free asymmetric 2bit quantization for kv cache," *arXiv preprint arXiv:2402.02750*, 2024.
- [21] Z. Liu, C. Zhao, F. Iandola, C. Lai, Y. Tian, I. Fedorov, Y. Xiong, E. Chang, Y. Shi, R. Krishnamoorthi *et al.*, "Mobilellm: Optimizing sub-billion parameter language models for on-device use cases," *arXiv preprint arXiv:2402.14905*, 2024.
- [22] AI-Meta, "Introducing llama: A foundational, 65-billion-parameter large language model," *Meta AI*, 2023.
- [23] H. Face, "Hugging Face: The AI community building the future. www.huggingface.co," 2024, (Accessed: Sep. 10, 2024).
- [24] R. Zellers, A. Holtzman, Y. Bisk, A. Farhadi, and Y. Choi, "Hellaswag: Can a machine really finish your sentence?" 2019. [Online]. Available: <https://arxiv.org/abs/1905.07830>
- [25] D. Hendrycks, C. Burns, S. Basart, A. Zou, M. Mazeika, D. Song, and J. Steinhardt, "Measuring massive multitask language understanding," *arXiv preprint arXiv:2009.03300*, 2020.
- [26] P. Clark, I. Cowhey, O. Etzioni, T. Khot, A. Sabharwal, C. Schoenick, and O. Tafjord, "Think you have solved question answering? try arc, the ai2 reasoning challenge," 2018. [Online]. Available: <https://arxiv.org/abs/1803.05457>
- [27] S. Lin, J. Hilton, and O. Evans, "Truthfulqa: Measuring how models mimic human falsehoods," 2021.
- [28] "Winogrande: An adversarial winograd schema challenge at scale," 2019.
- [29] S. Merity, C. Xiong, J. Bradbury, and R. Socher, "Pointer sentinel mixture models," *arXiv preprint arXiv:1609.07843*, 2016.
- [30] A. Chinchuluun and P. M. Pardalos, "A survey of recent developments in multiobjective optimization," *Annals of Operations Research*, vol. 154, no. 1, pp. 29–50, 2007.
- [31] S. Brisset and F. Gillon, "Approaches for multi-objective optimization in the ecodesign of electric systems," *Eco-friendly innovation in electricity transmission and distribution networks*, pp. 83–97, 2015.

- [32] G. Santoro, M. R. Casu, V. Peluso, A. Calimera, and M. Alioto, "Design-space exploration of pareto-optimal architectures for deep learning with dvfs," in *2018 IEEE International Symposium on Circuits and Systems (ISCAS)*. IEEE, 2018, pp. 1–5.



Dawar Khan earned his Ph.D. from the NLPRI, Institute of Automation, University of Chinese Academy of Sciences, Beijing, China, in 2018. He served as an Assistant Professor at the NAIST, Nara, Japan, from 2018 to 2020, and subsequently at the University of Haripur, Pakistan, until 2022. Since April 2022, he has been a Postdoctoral Fellow at KAUST in Saudi Arabia. His research interests encompass computer graphics, visualization, and augmented reality.



Xinyu Liu is currently a final-year undergraduate student in Internet of Things Engineering at the School of Information and Communication Engineering, University of Electronic Science and Technology of China (UESTC), China. In the summer of 2024, he participated in the Visiting Student Research Program (VSRP) at King Abdullah University of Science and Technology (KAUST). His research interests include IoT, XR development, and large language models.



Omar Mena is a PhD student in Computer Science under the supervision of Professor Ivan Viola at King Abdullah University of Science and Technology (KAUST). He obtained his BSc in Artificial Intelligence at Universidad Panamericana, Mexico, and his MSc in Computer Science from KAUST. His research interests are XR human-computer interaction and computer graphics.



Donggang Jia is a Computer Science PhD student at King Abdullah University of Science and Technology (KAUST), where he is part of the nanovisualization group. He received a B. Eng degree in Computer Science from the Beijing University of Posts and Telecommunications, China, and an MSc in Artificial Intelligence from the University of Southampton, UK. His research interests include scientific visualization, human-computer interaction, and computer graphics.



Alexandre Kouyoumdjian is a research scientist at King Abdullah University of Science and Technology (KAUST). He holds a PhD in computer science from University Paris-Saclay. He conducts research on multiscale visualization, interaction, and modeling for biology, with an additional focus on virtual and augmented reality.



Ivan Viola is a professor at King Abdullah University of Science and Technology, Saudi Arabia. He graduated from TU Wien, Austria. In 2005 he took a postdoc position at the University of Bergen, Norway, where he was gradually promoted to the professor rank. In 2013 he received a WWTF grant to establish a research group at TU Wien. At KAUST, he continues developing new visualization techniques, primarily oriented on data reconstruction, interpretation, representation, modeling, and rendering.